



Direct coating ZnO nanocrystals onto 1D Fe₃O₄/C composite microrods as highly efficient and reusable photocatalysts for water treatment



Yanrong Wang^{a,1}, Jiqiang Ning^{b,1}, Enlai Hu^a, Changcheng Zheng^{b,c}, Yijun Zhong^{a,*}, Yong Hu^{a,*}

^a Institute of Physical Chemistry, Zhejiang Normal University, Jinhua 321004, PR China

^b Department of Physics and HKU-CAS Joint Laboratory on New Materials, The University of Hong Kong, Pokfulam Road, Hong Kong, China

^c Mathematics and Physics Centre, Department of Mathematical Sciences, Xi'an Jiaotong-Liverpool University, Suzhou 215123, PR China

ARTICLE INFO

Article history:

Received 31 December 2014

Received in revised form 2 March 2015

Accepted 3 March 2015

Available online 10 March 2015

Keywords:

Composite microrods

ZnO nanocrystals

Core-shell nanostructure

Magnetic field-induced

Photodecolorization

ABSTRACT

In this work, we demonstrated a facile two-step method to directly coat a ZnO nanocrystal layer on the surface of one-dimensional (1D) Fe₃O₄/C composite microrods to form Fe₃O₄/C@ZnO core-shell microrods. Firstly, 1D Fe₃O₄/C composite microrods were successfully synthesized by one-pot magnetic field-induced solvothermal reaction according to our previous work. Secondly, a uniform ZnO nanocrystal layer was facilely coated onto the 1D Fe₃O₄/C composite microrods via a modified hydrothermal process at a low temperature (60 °C). Importantly, the size of ZnO nanocrystals and the thickness of coating layer can be easily tuned by varying the concentration of Zn(Ac)₂·2H₂O in the solution. Further investigation has revealed that the as-prepared core-shell microrods exhibited enhanced photocatalytic activity for the decolorization of photosensitized dyes (Congo red) under visible-light illumination. Moreover, these magnetically separable photocatalysts can be readily recycled by a magnet with virtually no loss in catalytic efficiency. We believe this facile synthesis strategy provides a general and efficient way to synthesize other 1D magnetic nanocomposites for different functional applications.

© 2015 Elsevier B.V. All rights reserved.

1. Introduction

Photocatalytic degradation of toxic organic compounds by semiconductor nanomaterials using inexhaustible solar energy has become a modern water treatment technology in recent years [1]. However, the separation of photocatalysts from large volumes of reaction solution remains a challenge in practical applications. Therefore, it is highly desirable to develop a reliable approach for realization of photocatalyst recycling [2,3]. Fortunately, magnetic materials can be collected easily by an external magnetic field, which can act as a carrier to facilitate material separation and recycling in aqueous solutions [4–6]. Therefore, the combination of photocatalysts and magnetic materials has an advantageous prospect in the photodegradation process [7–10]. In order to protect the magnetic particles from chemical degradation or agglomeration in practical applications, it is necessary to coat the magnetic material with an organic or inorganic shell [11,12]. Because the surface of the amorphous carbon is hydrophilic and has abundant amounts of –OH and –COO[–] groups, which can bind metal cations

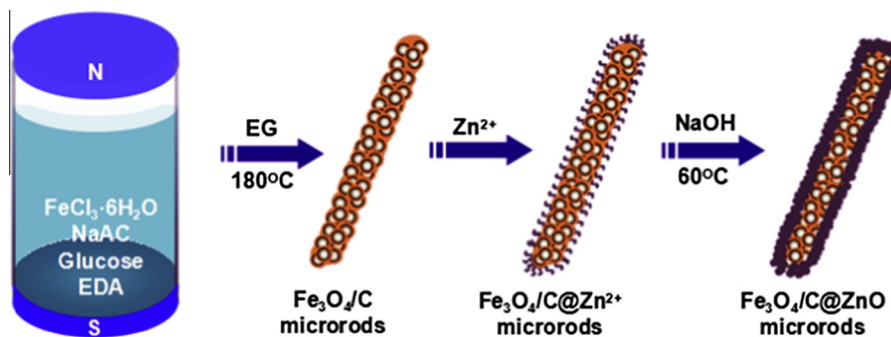
through coordination or electrostatic interactions in solution [13]. Therefore, amorphous carbon can be used as unique coating or supporting material for different applications [14–16].

Very recently, we have successfully synthesized 1D magnetic Fe₃O₄/C composite microrods by a one-pot magnetic field-induced solvothermal method, which demonstrate much better lithium storage properties than Fe₃O₄ nanospheres [17]. Considering the requirement of photocatalysts in practical applications, these 1D magnetic Fe₃O₄/C composite microrods can offer multifold advantages: (a) introduction of additional functionalities due to the presence of abundant surface reactive groups, which can act as an excellent supporting material to bind other semiconductor photocatalysts for realization of rapid recycling [18]. (b) The magnetic component might not only prevent the agglomeration of the catalyst nanocrystals during recovery, but also offer some synergetic enhancement of the catalytic activity by forming the hybrid structure [19]. (c) 1D nanostructures with the unique structure of anisotropy, low dimension and enhanced aspect ratio, are considered to be beneficial for photocatalytic and electrochemical performance since they facilitate electron and ion transport [20–22]. (d) The presence of amorphous carbon in 1D magnetic Fe₃O₄/C microrods not only promotes the absorption of light, but also accelerates the electron transfer, thus improving the photocatalytic efficiency [23].

* Corresponding authors. Tel.: +86 579 82282234; fax: +86 579 82282595.

E-mail address: yonghu@zjnu.edu.cn (Y. Hu).

¹ These authors contributed equally to this work.



Scheme 1. Schematic illustration of the formation of 1D $\text{Fe}_3\text{O}_4/\text{C}@\text{ZnO}$ core-shell composite microrods.

As one of the most important multifunctional semiconductor materials, ZnO has been widely noted and studied due to their low-cost, high quantum efficiency and high photocatalytic activity and stability [24–29]. Because the synthetic methods of ZnO nano/micro-structures are usually simple, low-temperature, non-toxic, environmentally-friendly [30–36], ZnO has been regarded as a promising photocatalytic material for realizing commercialization. In this study, as a proof-of-concept demonstration of the functional properties of the as-prepared 1D $\text{Fe}_3\text{O}_4/\text{C}$ composite microrods, we choose ZnO nanocrystal as a coating layer to form $\text{Fe}_3\text{O}_4/\text{C}@\text{ZnO}$ core-shell microrods, which exhibit obviously enhanced photocatalytic activity and excellent recyclability for the decolorization of photosensitized dye Congo red (CR) under visible-light illumination.

The detailed synthesis process is schematically demonstrated in Scheme 1. Firstly, 1D $\text{Fe}_3\text{O}_4/\text{C}$ composite microrods were synthesized by one-pot magnetic-field inducing solvothermal method [17]. Secondly, a uniform ZnO nanocrystal layer was deposited on the surface of 1D $\text{Fe}_3\text{O}_4/\text{C}$ microrods through a facile modified hydrothermal process, which only requires $\text{Zn}(\text{Ac})_2 \cdot 2\text{H}_2\text{O}$ and NaOH as reagents reacting at 60 °C for 2 h in water. It is found that the size of ZnO nanocrystals and the thickness of shell layer can also be tuned by varying the concentration of precursors. Furthermore, the 1D $\text{Fe}_3\text{O}_4/\text{C}@\text{ZnO}$ core-shell microrods not only exhibit excellent photocatalytic activity for the decolorization of CR under visible-light irradiation, but also can be readily recycled by a simple magnet with virtually no loss in catalytic efficiency. Therefore, this design provides a promising candidate for removing toxic organic pollutants during water treatment process.

2. Experimental details

All reagents were analytical grade, purchased from the Shanghai Chemical Reagent Factory, and used as received without further purification.

2.1. Synthesis of 1D $\text{Fe}_3\text{O}_4/\text{C}$ composite microrods

1D $\text{Fe}_3\text{O}_4/\text{C}$ microrods were prepared according to our previous work [17]. Briefly, 0.4 g of $\text{FeCl}_3 \cdot 6\text{H}_2\text{O}$ and 0.3 g of NaAc were dispersed into a mixed solvent of 15 mL of ethylene glycol and 3 mL of ethylenediamine with the assistance of ultrasonication. Then, 0.4 g of glucose was added into the above suspension, and the resulting mixture was transferred into a 20 mL of Teflon-lined stainless steel autoclave in the presence of an external magnetic field (0.2 T), and heated at 180 °C for 6 h. Finally, the as-obtained $\text{Fe}_3\text{O}_4/\text{C}$ composite microrods were collected and washed with distilled water and ethanol for several times by centrifugation, then dried in an oven at 60 °C for 6 h.

2.2. Synthesis of 1D $\text{Fe}_3\text{O}_4/\text{C}@\text{ZnO}$ core-shell microrods

In a typical procedure, a certain amount of $\text{Zn}(\text{Ac})_2 \cdot 2\text{H}_2\text{O}$ was added into 20 mL of distilled water to form a clear solution. 50 mg of $\text{Fe}_3\text{O}_4/\text{C}$ composite microrods was added to the above solution with the assistance of sonication for 10 min. Subsequently, the mixture was stirred by a mechanical stirring, followed by heating at 60 °C for 2 h to allow the Zn^{2+} ions fully interact with the surface functional

Table 1

Control of ZnO particle size in 1D $\text{Fe}_3\text{O}_4/\text{C}@\text{ZnO}$ composite microrods using different Zn^{2+} concentrations.

Sample	Zn^{2+} concentration/ M	NaOH concentration/ M	ZnO particle size/ nm^a
Sa	0.0031	0.0063	9.0
Sb	0.0063	0.0125	11.1
Sc	0.0125	0.0250	13.7
Sd	0.0250	0.0500	17.6

^a ZnO particle size was calculated from XRD diffraction data.

groups (e.g., carboxylic) of the $\text{Fe}_3\text{O}_4/\text{C}$ composites. Then, 5 mL of NaOH aqueous solution was dropwise added and kept stirring at 60 °C for 2 h. Finally, the product was collected by a magnet, and washed with distilled water and ethanol for several times, then dried in an oven at 60 °C for 6 h. In order to optimize the properties of the 1D $\text{Fe}_3\text{O}_4/\text{C}@\text{ZnO}$ core-shell microrods for photocatalytic applications, different concentrations of $\text{Zn}(\text{Ac})_2 \cdot 2\text{H}_2\text{O}$ and also corresponding NaOH were used, while the other conditions remain unchanged. Products prepared with different concentrations of $\text{Zn}(\text{Ac})_2 \cdot 2\text{H}_2\text{O}$ (0.0031, 0.0063, 0.0125 and 0.0250 M) by seeding and growth process were assigned to sample codes Sa, Sb, Sc and Sd, respectively (see Table 1).

2.3. Characterization

Powder X-ray diffraction (XRD) measurements of the samples were performed with a Philips PW3040/60 X-ray diffractometer using Cu K α radiation at a scanning rate of 0.06°s⁻¹. Scanning electron microscopy (SEM) images were obtained by a Hitachi S-4800 scanning electron microanalyzer with an accelerating voltage of 15 kV. Transmission electron microscopy (TEM) and high-resolution transmission electron microscopy (HRTEM) were conducted at 200 kV with a JEM-2100F field emission TEM. Further evidence for the composition of the products was inferred from X-ray photoelectron spectroscopy (XPS), using an ESCALab MKII X-ray photoelectron spectrometer with Mg K α X-ray as the excitation source. The absorption spectra were measured using a PerkinElmer Lambda 900 UV–vis spectrophotometer at room temperature.

2.4. Photocatalytic activity measurement

Photocatalytic activities of the as-prepared 1D $\text{Fe}_3\text{O}_4/\text{C}@\text{ZnO}$ core-shell composite microrods were evaluated by the degradation of CR under visible-light irradiation from a 500 W Xe lamp (CEL-HXF300) with a 420 nm cut off filter. The reaction cell was placed in a sealed black box with the top opened, and the cut off filter was placed to provide visible-light irradiation. In a typical process, 20 mg of as-prepared photocatalysts was added into 20 mL of CR solution (concentration: 100 mg L⁻¹). After being dispersed in an ultrasonic bath for 5 min, the solution was stirred for 2 h in the dark to reach adsorption equilibrium between the catalyst and the solution and then exposed to visible-light irradiation. The samples were collected by a magnet at given time intervals to measure the CR concentration by UV–vis spectroscopy. To further study the recyclability of the 1D $\text{Fe}_3\text{O}_4/\text{C}@\text{ZnO}$ core-shell composite microrods, we also examined the photocatalytic activity of sample Sd for 10 rounds. The recycled photocatalyst sample was reused without any post-treatment except being washed with ethanol and distilled water three times after each photocatalytic degradation of CR.

·OH radical reactions were performed as follows. 5 mg of each 1D $\text{Fe}_3\text{O}_4/\text{C}@\text{ZnO}$ core-shell composite microrods with different ZnO nanocrystal sizes were suspended in 10 mL of aqueous solution containing 100 mg L⁻¹ of CR, 10 mM of NaOH and 5 mM of terephthalic acid (TA), respectively. Before exposure to visible-light, the suspension was stirred in the dark for 10 min. After irradiated for 10 min, the products were collected by a magnet, and the rest

of solution was collected for fluorescence spectroscopy measurements. A fluorescence spectrophotometer was then used to measure the fluorescence signal of the generated 2-hydroxy-terephthalic acid (TAOH). The excitation light wavelength used in recording fluorescence spectra was 320 nm.

3. Results and discussion

The crystallographic structure and phase purity of the as-prepared 1D $\text{Fe}_3\text{O}_4/\text{C}/\text{ZnO}$ core-shell microrods were examined by XRD measurements. As shown in Fig. 1, the diffraction peaks in the XRD patterns marked with empty triangles can be assigned to face-centered cubic magnetite Fe_3O_4 (JCPDS standard card No. 19-0629. $a = 8.396 \text{ \AA}$). Other diffraction peaks marked with asterisks can be well indexed to hexagonal phase of ZnO (JCPDS standard card No. 36-1451. $a = b = 3.250 \text{ \AA}$ and $c = 5.207 \text{ \AA}$). Because the (440) diffraction peak of Fe_3O_4 is very adjacent to the (103) diffraction peak of ZnO, two peaks are overlapped together. With increasing amount of Zn^{2+} ion, the diffraction intensity of the strongest ZnO (100) peak increases gradually, indicating that the ZnO nanocrystals grow larger with better crystallinity. The corresponding particle sizes of ZnO with the different Zn^{2+} concentrations are listed in Table 1, which confirming that the ZnO nanoparticles grow larger with better crystallinity. In addition, the XRD pattern of the 1D $\text{Fe}_3\text{O}_4/\text{C}$ composite microrods is shown in Fig. 2a.

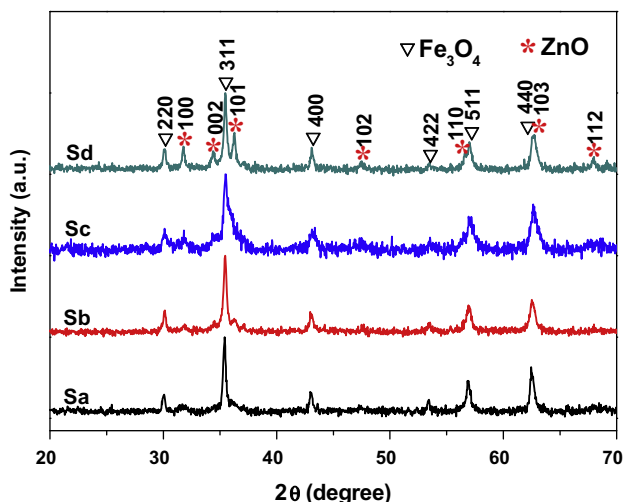


Fig. 1. XRD patterns of as-prepared 1D $\text{Fe}_3\text{O}_4/\text{C}/\text{ZnO}$ core-shell composite microrods loaded with different amounts of ZnO, denoted as Sa, Sb, Sc, and Sd, respectively.

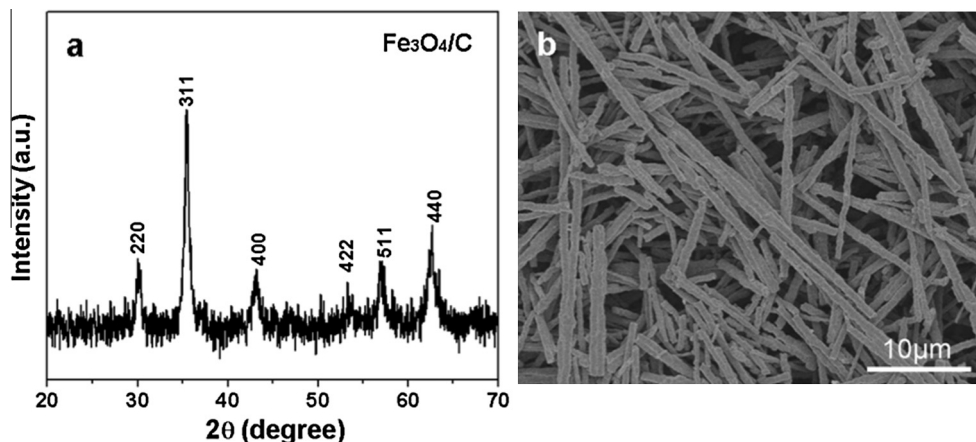


Fig. 2. XRD pattern (a) and SEM image and (b) of the 1D $\text{Fe}_3\text{O}_4/\text{C}$ composite microrods.

The SEM images of the as-prepared 1D $\text{Fe}_3\text{O}_4/\text{C}/\text{ZnO}$ core-shell microrods synthesized with the different $\text{Zn}(\text{AC})_2$ concentrations are shown in Fig. 3. These images depict microrods with nearly uniform size, about 1–1.5 μm in diameter and several micrometers in length. Besides, the rod morphology of all samples is well preserved without any observable impurity particles or aggregates. With increasing the concentration of Zn^{2+} , obvious changes of the microrod surface can be observed from Fig. 3a–d. Specifically, the size of ZnO nanocrystals on the surface of 1D $\text{Fe}_3\text{O}_4/\text{C}$ microrods becomes larger and the diameter of 1D $\text{Fe}_3\text{O}_4/\text{C}/\text{ZnO}$ core-shell microrods increases gradually. For comparison, the SEM image of 1D $\text{Fe}_3\text{O}_4/\text{C}$ composite microrods was shown in Fig. 2b. It is clearly seen that the surface of 1D $\text{Fe}_3\text{O}_4/\text{C}/\text{ZnO}$ core-shell composite microrods was rougher than that of the 1D $\text{Fe}_3\text{O}_4/\text{C}$ composite microrods.

Further morphology and structure characterizations of the as-prepared samples are elucidated by TEM observation. Fig. 4a–d shows the typical TEM images of 1D $\text{Fe}_3\text{O}_4/\text{C}/\text{ZnO}$ core-shell microrods loaded with different amounts of ZnO, respectively. The inset in Fig. 4a shows the HRTEM of sample Sa, which demonstrates that the ZnO coating layer is successfully deposited on the surface of 1D $\text{Fe}_3\text{O}_4/\text{C}$ microrods. From the HRTEM image (the inset in Fig. 4d), clear lattice fringes of ZnO coating layer can be observed and match well with hexagonal phase of ZnO with lattice spacing at 0.25 nm and 0.28 nm corresponding to the (101) planes and (100) plane of ZnO. From all TEM images, it can be clearly seen that ZnO coating layer was uniformly deposited on the surface of 1D $\text{Fe}_3\text{O}_4/\text{C}$ microrods, and the thickness of ZnO coating layer increases gradually with increasing the concentration of precursors. The thickness of ZnO coating layer of Sa, Sb, Sc, and Sd are about 25 nm, 45 nm, 110 nm and 200 nm, respectively. These results are in good agreement with the XRD and SEM analyses.

Additionally, the chemical states of elements in the 1D $\text{Fe}_3\text{O}_4/\text{C}/\text{ZnO}$ core-shell composite microrods are further studied by the XPS technique. A typical survey spectrum of the 1D $\text{Fe}_3\text{O}_4/\text{C}/\text{ZnO}$ composite microrods is depicted in Fig. S1 (see the Supporting Information), which displays the presence of O, C, Zn, and Fe elements. Fig. 5a displays a high-resolution spectrum of Zn, the peaks at 1021.0 eV and 1044.0 eV correspond to Zn 2p_{3/2} and 2p_{1/2}, respectively [37]. In the spectrum of Fe2p (Fig. 5b), the Fe2p_{3/2} and Fe2p_{1/2} peaks are located at 710.3 and 724.0 eV respectively. The characteristic satellite peak at 719.0 eV of $\alpha\text{-Fe}_2\text{O}_3$ or $\gamma\text{-Fe}_2\text{O}_3$ is not observed [38–40], indicating the pure Fe_3O_4 phase in 1D $\text{Fe}_3\text{O}_4/\text{C}/\text{ZnO}$ core-shell microrods. Fig. 5c shows a high-resolution spectrum of O 1s, which can be deconvoluted into three peaks by the XPS peak fitting program. The peaks

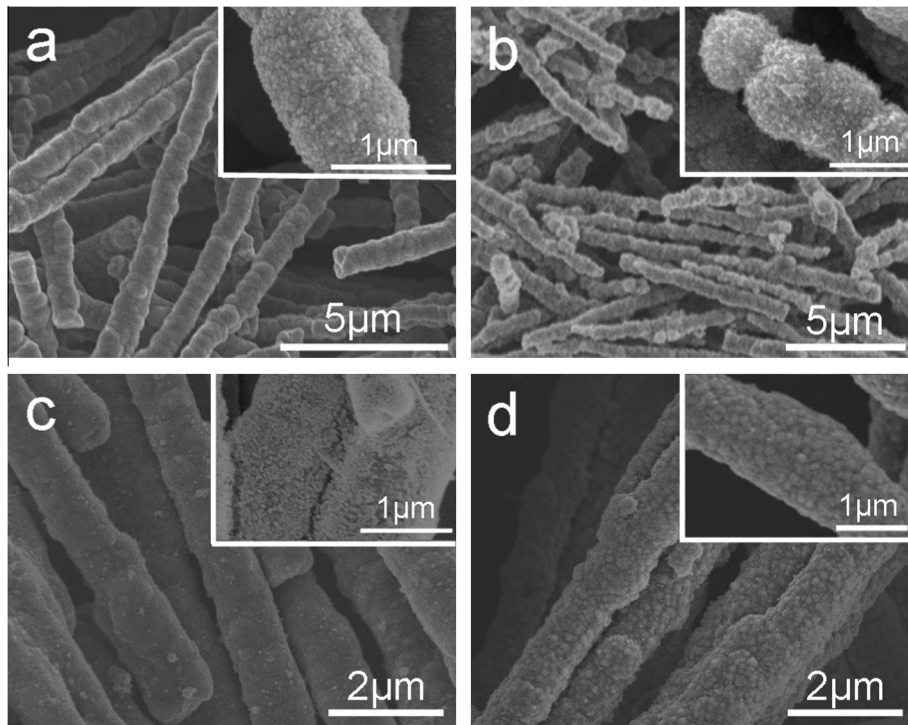


Fig. 3. Sem images of as-prepared 1D $\text{Fe}_3\text{O}_4/\text{C}@\text{ZnO}$ core-shell composite microrods loaded with different amounts of ZnO, (a) Sa, (b) Sb, (c) Sc and (d) Sd.

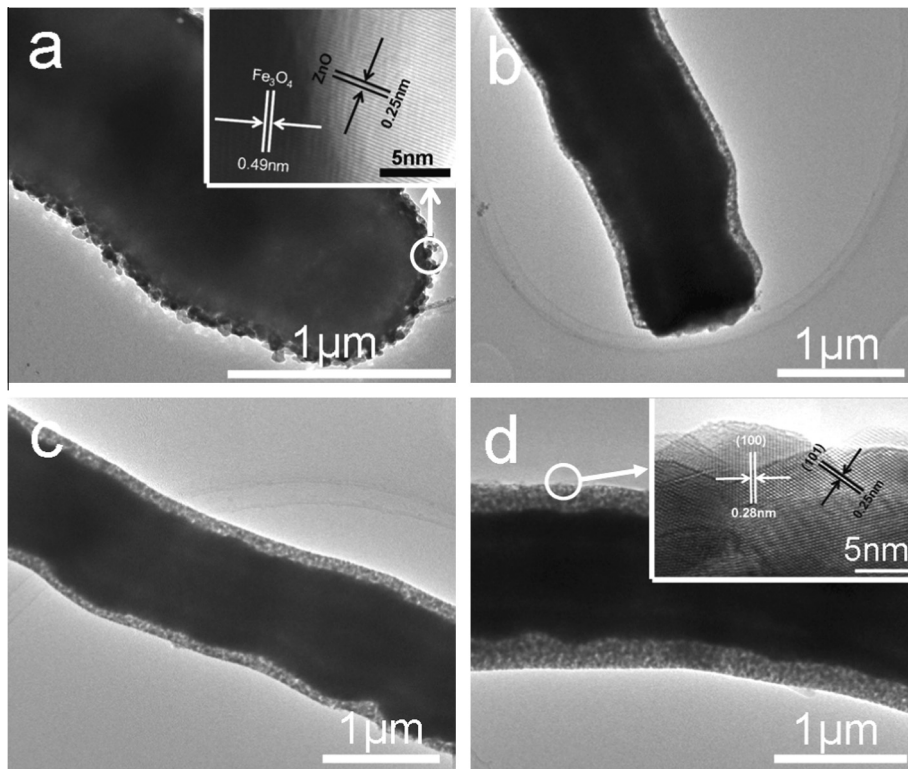


Fig. 4. TEM images of as-prepared 1D $\text{Fe}_3\text{O}_4/\text{C}@\text{ZnO}$ composite microrods loaded with different amounts of ZnO, (a) Sa, (b) Sb, (c) Sc and (d) Sd.

at 530.2 and 531.9 eV can be attributed to O in Fe_3O_4 and ZnO, respectively [41,42]. The peak at 531.0 is associated with the O^{2-} ions in the oxygen-deficient regions within the ZnO matrix [43]. The high-resolution spectrum of C1s is displayed in Fig. 5d, which

also can be resolved into three peaks. The core level spectrum in the C1s region displays an asymmetric broad peak, which indicates that more than one chemical states of C are present [44]. By fitting the experimental line profile, three peaks are identified and

assigned to the aliphatic C–C bond (284.7 eV), O–C–O complex (286.1 eV), and carbonate species (288.5 eV) [23,45]. The higher binding energy suggests the carbon may be incorporating into the interstitial positions of the Fe_3O_4 lattice, and also the possibly of such defect complexes that involve C–O bonds [38,46].

The photocatalytic activities of the as-prepared 1D $\text{Fe}_3\text{O}_4/\text{C}@\text{ZnO}$ core-shell microrods were evaluated by the decolorization of CR in water. Fig. 6a displays the decolorization behavior of CR in the absence of any photocatalyst (that is, the blank test), in the presence of commercial ZnO powder, the as-prepared 1D $\text{Fe}_3\text{O}_4/\text{C}$ composite microrods and 1D $\text{Fe}_3\text{O}_4/\text{C}@\text{ZnO}$ core-shell microrods after exposure to visible-light irradiation, where C is the concentration of CR after different light irradiation time intervals and C_0 is the initial concentration of the CR before dark adsorption. After visible light irradiation for 60 min, approximately 59.8% of CR is decolorized using commercial ZnO as the photocatalyst, while 17.8% of CR is decolorized in the presence of 1D $\text{Fe}_3\text{O}_4/\text{C}$ microrods. The decolorization fractions using 1D $\text{Fe}_3\text{O}_4/\text{C}@\text{ZnO}$ composite microrods (Sa, Sb, Sc and Sd) as photocatalysts are about 60.4, 70.5%, 81.5%, and 96.7%, respectively. This result indicates that the decolorization efficiency enhanced by increasing loading amount of ZnO is more active than commercial ZnO. The particle size of commercial ZnO powder is about 41.8 nm estimated using the Debye–Scherrer equation according to our previous work [35]. Thus, the enhanced decolorization efficiency of the as-prepared 1D $\text{Fe}_3\text{O}_4/\text{C}@\text{ZnO}$ core-shell composite microrods may be ascribed to the unique 1D microrod structure and the presence of amorphous carbon, both of which could accelerate the transport of electrons, promoting the separation of photogenerated charges, as well as the dispersion of composite microrods in an aqueous solution allowing more reactive sites for adsorption and decolorization of CR [47]. The reusability of the 1D $\text{Fe}_3\text{O}_4/\text{C}@\text{ZnO}$

composite microrods as photocatalysts was also investigated by collecting and reusing the same photocatalyst for multiple cycles. As shown in Fig. 6b, where the sample Sd was used for the reusability test, the photocatalytic activity does not show significant loss up to 10 cycles of photo-decolorization of CR dye, indicating the excellent stability of samples. Furthermore, the magnetic recyclable photocatalysts are also favorable because of the great ease in separation from the reaction solution by a magnet after each degradation reaction. Thus, the results suggest that the magnetic 1D $\text{Fe}_3\text{O}_4/\text{C}@\text{ZnO}$ core-shell composite microrods are stable and have great application potential in water treatment.

We speculate that the decolorization of dyes is mainly due to the photosensitization process because that ZnO has no apparent absorption in the visible-light region. Dye rather than ZnO is excited by visible light to form excited Dye (Dye*). Dye* can directly inject electrons into the conduction band of ZnO semiconductor, forming conduction band electrons, the electron is trapped by surface adsorbed O_2 to generate various reactive oxidative species (ROSSs), the dye* subsequently self-degrades or is degraded by ROSSs. Thus, the decolorization efficiency greatly depends on the electron transfer between the dye* and the as-prepared nanohybrids [24,35,48,49]. The relative band edge alignment of different components was illustrated in Fig.S2 (see the Supporting Information).

In this hybrid structure, the electrons in the conduction band of ZnO can easily transfer to 1D $\text{Fe}_3\text{O}_4/\text{C}$ microrods, which contribute to improve effective separation of electrons and holes. Additionally, 1D $\text{Fe}_3\text{O}_4/\text{C}$ microrod is believed to be beneficial for achieving higher photocatalytic performance since it facilitates electron transport [50]. To verify this speculation, we measure the $\cdot\text{OH}$ radicals formed in different 1D $\text{Fe}_3\text{O}_4/\text{C}@\text{ZnO}$ core-shell microrods obtained with different $\text{Zn}(\text{AC})_2$ concentrations

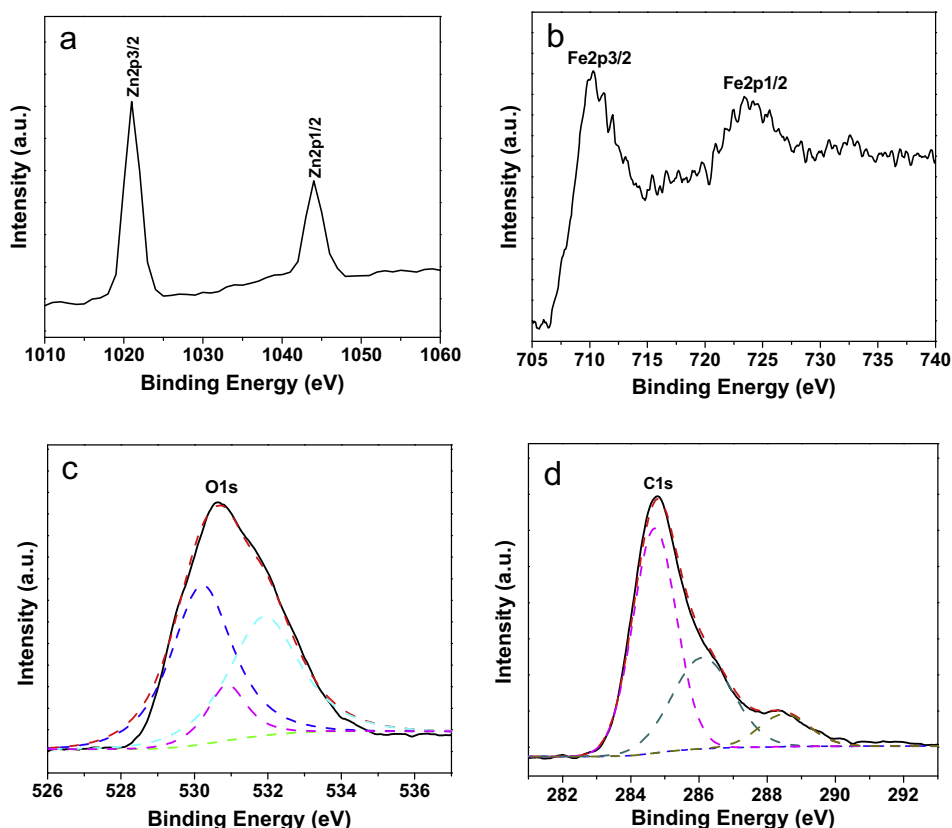


Fig. 5. XPS spectra of as-prepared 1D $\text{Fe}_3\text{O}_4/\text{C}@\text{ZnO}$ core-shell composite microrods: (a) Zn2p spectrum, (b) Fe2p spectrum, (c) O1s spectrum and (d) C1s spectrum.

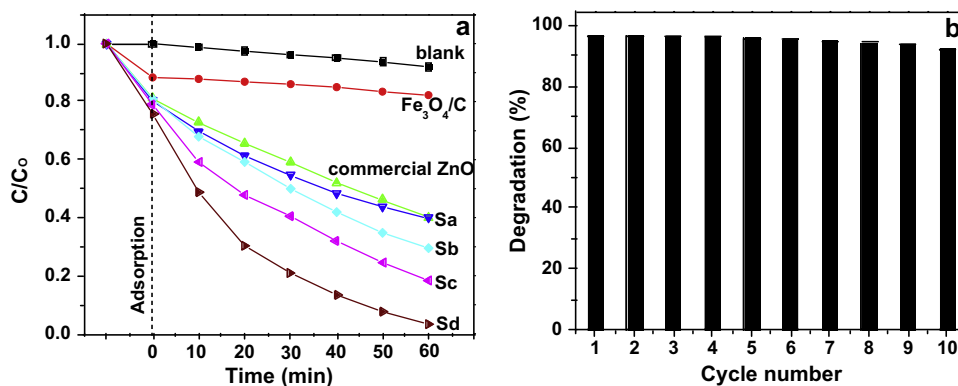


Fig. 6. (a) Photocatalytic degradation of CR in the absence of any photocatalyst (the blank test), with 1D Fe₃O₄/C microrods, commercial ZnO and in the presence of 1D Fe₃O₄/C@ZnO core-shell composite microrods loaded with different amounts of ZnO: (a) Sa, (b) Sb, (c) Sc and (d) Sd. (b) 10 cycles of the degradation of CR using sample Sd as the photocatalyst under visible light irradiation for 60 min.

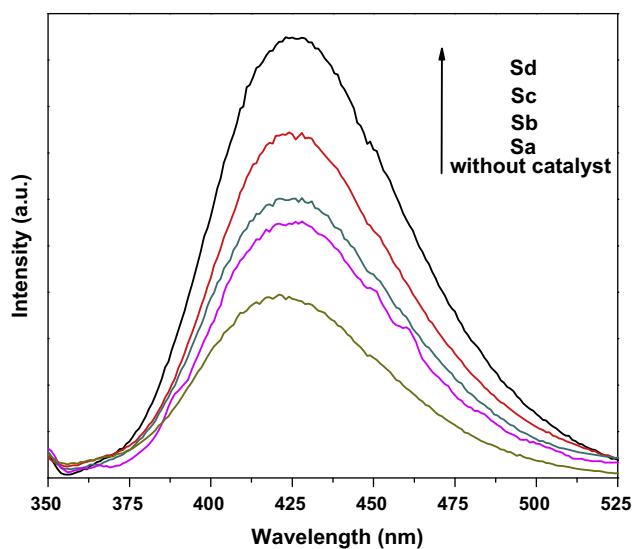


Fig. 7. Fluorescence spectra of TAOH formed by the reaction of TA with ·OH radicals generated from different samples (Sa, Sb, Sc and Sd) compared with no catalyst under visible-light irradiation for 10 min.

compared to that without catalysts in the presence of CR using a similar method described previously, which can be used to demonstrate the separation efficiency of photogenerated electrons and holes in the hybrid system [51]. It is well known that ·OH reacts with terephthalic acid (TA) in basic solution to generate 2-hydroxy-terephthalic acid (TAOH), which emits a unique fluorescence signal with the peak centered at 426 nm [52]. Significant fluorescent signals associated with TAOH are generated upon visible-light irradiation of the different photocatalysts suspended, and no catalysts in a TA solution in the presence of CR for 10 min. As shown in Fig. 7, it can be seen that ·OH radicals are formed in the solution with different photocatalysts in presence of CR in the photoreaction process under visible light irradiation. Obviously, fluorescence intensity increases with increasing loading amount of ZnO. When there is only CR in a TA solution, the emission peak of TAOH could also be observed, but it is much weaker than those of in the presence of 1D Fe₃O₄/C@ZnO core-shell microrods. Furthermore, the most ·OH radicals are formed using sample Sd in the decolorization process, and this result is in a good agreement with that of decolorization of dyes. In order to investigate the effect of IR light on photocatalytic activity, we used IR light (890–1500 nm) in the photocatalytic experiment, and the result

was shown in Fig. S3 (see Supporting Information). After IR light irradiation for 60 min, approximately 5% of CR is decolorized using 1D Fe₃O₄/C@ZnO core-shell composite microrods as the photocatalyst, which indicates that the effect of IR on photocatalytic activity can be negligible.

4. Conclusions

In summary, a facile two-step method has been developed to prepare 1D Fe₃O₄/C@ZnO core-shell microrods through a magnetic field-induced solvothermal route followed by a modified hydrothermal process. Importantly, the size of ZnO nanocrystals and the thickness of coating layer can be conveniently controlled by varying the concentration of Zn²⁺ during the synthesis process. These 1D Fe₃O₄/C@ZnO core-shell microrods exhibit excellent photostability and enhanced photodecolorization of CR dye under visible-light irradiation. The superior visible-light photocatalytic activity may be attributed to the unique 1D microrods structure and the presence of amorphous carbon, both of which could accelerate the transport of electrons, promoting the separation of photogenerated charges. We believe this facile synthesis method can be extended to produce other 1D magnetic nanocomposites containing 1D magnetic-carbon structure as the support and an outer layer of active nanomaterials for different applications.

Acknowledgements

Financial support from the Natural Science Foundation of China (21171146, 21371152) and Zhejiang Provincial Natural Science Foundation of China (LR14B010001, LR12B040001) are gratefully acknowledged.

Appendix A. Supplementary material

Supplementary data associated with this article can be found, in the online version, at <http://dx.doi.org/10.1016/j.jallcom.2015.03.033>.

References

- [1] S. Sakthivel, B. Neppolian, M.V. Shankar, B. Arabindoo, M. Palanichamy, V. Murugesan, *Sol. Energy Mater. Sol. C* 77 (2003) 65–82.
- [2] L. Zhang, W.Z. Wang, M. Shang, S.M. Sun, J.H. Xu, *J. Hazard. Mater.* 172 (2009) 1193–1197.
- [3] E.L. Hu, X.H. Gao, A. Etogo, Y.L. Xie, Y.J. Zhong, Y. Hu, *J. Alloys Comp.* 611 (2014) 335–340.
- [4] A.H. Lu, W. Schmidt, N. Matoussevitch, H. Bonnemann, B. Spliethoff, B. Tesche, E. Bill, W. Kiefer, F. Schuth, *Angew. Chem. Int. Ed.* 43 (2004) 4303–4306.

- [5] X.W. Lou, L.A. Archer, *Adv. Mater.* 20 (2008) 1853–1858.
- [6] C.P. Chen, P. Gunawan, R. Xu, *J. Mater. Chem.* 21 (2011) 1218–1225.
- [7] J.S. Chen, C.P. Chen, J. Liu, R. Xu, S.Z. Qiao, X.W. Lou, *Chem. Commun.* 47 (2011) 2631–2633.
- [8] L. Zhang, W.Z. Wang, L. Zhou, M. Shang, S.M. Sun, *Appl. Catal. B Environ.* 90 (2009) 458–462.
- [9] Z.H. Wang, S.Y. Zhu, S.P. Zhao, H.B. Hu, *J. Alloys Comp.* 509 (2011) 6893–6898.
- [10] A. Amarjargal, Z. Jiang, L.D. Tijing, C.H. Park, I. Imc, C.S. Kim, *J. Alloys Comp.* 580 (2013) 143–147.
- [11] Y. Deng, D. Qi, C. Deng, X. Zhang, D. Zhao, *J. Am. Chem. Soc.* 130 (2008) 28–29.
- [12] M.M. Ye, Q. Zhang, Y.X. Hu, J.P. Ge, Z.D. Lu, L. He, Z.L. Chen, Y.D. Yin, *Chem.-Eur. J.* 16 (2010) 6243–6250.
- [13] X.M. Sun, Y.D. Li, *Angew. Chem. Int. Ed.* 43 (2004) 597–601.
- [14] L. Zhang, G.Q. Zhang, H.B. Wu, L. Yu, X.W. Lou, *Adv. Mater.* 25 (2013) 2589–2593.
- [15] Y. Hu, X.H. Gao, L. Yu, Y.R. Wang, J.Q. Ning, S.J. Xu, X.W. Lou, *Angew. Chem. Int. Ed.* 52 (2013) 5636–5639.
- [16] W.L. Yang, Y.R. Wang, A. Etogo, J.Q. Ning, Y.L. Xie, H.u. Yong, *Nanoscale* 6 (2014) 3051–3054.
- [17] Y.R. Wang, L. Zhang, X.H. Gao, L.Y. Mao, Y. Hu, X.W. Lou, *Small* 10 (2014) 2815–2819.
- [18] Y. Liu, L. Zhou, Y. Hu, C.F. Guo, H.S. Qian, F.M. Zhang, X.W. Lou, *J. Mater. Chem.* 21 (2011) 18359–18364.
- [19] L. Wang, H.W. Wei, Y.J. Fan, X. Gu, J.H. Zhan, *J. Phys. Chem. C* 113 (2009) 14119–14125.
- [20] W.L. Yang, L. Zhang, Y. Hu, Y.J. Zhong, H.B. Wu, X.W. Lou, *Angew. Chem. Int. Ed.* 51 (2012) 11501–11504.
- [21] Y.R. Wang, W.L. Yang, L. Zhang, Y. Hu, X.W. Lou, *Nanoscale* 5 (2013) 10864–10867.
- [22] N. Kang, J.H. Park, J. Choi, J. Jin, J. Chun, I.G. Jung, J. Jeong, J.G. Park, S.M. Lee, H.J. Kim, S.U. Son, *Angew. Chem. Int. Ed.* 51 (2012) 6626–6630.
- [23] M.J. Zhou, X.H. Gao, Y. Hu, J.F. Chen, X. Hu, *Appl. Catal. B Environ.* 138–139 (2013) 1–8.
- [24] Y. Liu, Y. Hu, M.J. Zhou, H.S. Qian, X. Hu, *Appl. Catal. B Environ.* 125 (2012) 425–431.
- [25] P. Li, Z. Wei, T. Wu, Q. Peng, Y.D. Li, *J. Am. Chem. Soc.* 133 (2011) 5660–5663.
- [26] Y. Hu, H.H. Qian, Y. Liu, G.H. Du, F.M. Zhang, L.B. Wang, X. Hu, *CrystEngComm* 13 (2011) 3438–3443.
- [27] Y.Q. Zhu, G.T. Fei, Y. Zhang, X.M. Chen, H.B. Tang, L.D. Zhang, *J. Phys. Chem. C* 115 (2011) 13597–13602.
- [28] P. Rai, H.M. Song, Y.S. Kim, M.K. Song, P.R. Oh, J.M. Yoon, Y.T. Yu, *Mater. Lett.* 68 (2012) 90–93.
- [29] J. Gupta, K.C. Barick, D. Bahadur, *J. Alloys Comp.* 509 (2011) 6725–6730.
- [30] U.N. Maiti, S.F. Ahmed, M.K. Mitra, K.K. Chattopadhyay, *Mater. Res. Bull.* 44 (2009) 134–139.
- [31] J.X. Wang, X.W. Sun, Y. Yang, H. Huang, Y.C. Lee, O.K. Tan, L. Vaussieres, *Nanotechnology* 17 (2006) 4995–4998.
- [32] K.S. Kim, H. Jeong, M.S. Jeong, G.Y. Jung, *Adv. Funct. Mater.* 20 (2010) 3055–3063.
- [33] S. Singh, K.C. Barickm, D. Bahadur, *J. Mater. Chem. A* 1 (2013) 3325–3333.
- [34] Y.J. Chen, F. Zhang, G.G. Zhao, X.Y. Fang, H.B. Jin, P. Gao, C.L. Zhu, M.S. Cao, G. Xiao, *J. Phys. Chem. C* 114 (2010) 9239–9244.
- [35] Y. Liu, L. Yu, Y. Hu, C.F. Guo, F.M. Zhang, X.W. Lou, *Nanoscale* 4 (2012) 183–187.
- [36] Y.L. Fang, Z.Y. Li, S. Xu, D.D. Han, D.Y. Lu, *J. Alloys Comp.* 575 (2013) 359–363.
- [37] Y. Hong, C.G. Tian, B.J. Jiang, A.P. Wu, Q. Zhang, G.H. Tian, H.G. Fu, *J. Mater. Chem. A* 1 (2013) 5700–5708.
- [38] Y.J. Ye, J. Chen, Q.Q. Ding, D.Y. Lin, R.L. Dong, L.B. Yang, J.H. Liu, *Nanoscale* 5 (2013) 5887–5895.
- [39] R.P. Ji, J.S. Jiang, M. Hu, *J. Phys. Chem. C* 114 (2010) 12090–12094.
- [40] C.N. He, S. Wu, N.Q. Zhao, C.S. Shi, E.Z. Liu, J.J. Li, *ACS Nano* 7 (2013) 4459–4469.
- [41] X.P. Dong, H.R. Chen, W.R. Zhao, X. Li, J.L. Shi, *Chem. Mater.* 19 (2007) 3484–3490.
- [42] N.M. Bahadur, T. Furusawa, M. Sato, F. Kurayama, N. Suzuki, *Mater. Res. Bull.* 45 (2010) 1383–1388.
- [43] Q. Zhu, C.S. Xie, H.Y. Li, C.Q. Yang, S.P. Zhang, D.W. Zeng, *J. Mater. Chem. C* 2 (2014) 4566–4580.
- [44] S. Cho, J.W. Jang, J.S. Lee, K.H. Lee, *CrystEngComm* 12 (2010) 3929–3935.
- [45] V. Chandra, J. Park, Y. Chun, J.W. Lee, I.C. Hwang, K.S. Kim, *ACS Nano* 4 (2010) 3979–3986.
- [46] S.H. Xuan, L.Y. Hao, W.Q. Jiang, X.L. Gong, Y. Hu, Z.Y. Chen, *Nanotechnology* 18 (2007) 35602–35607.
- [47] X.Y. Cai, B.Q. Han, S.J. Deng, Y. Wang, C.J. Dong, Y.D. Wang, I. Djerdj, *CrystEngComm* 16 (2014) 7761–7770.
- [48] A. Dolbecq, P. Mialane, B. Keitab, L. Nadjo, *J. Mater. Chem.* 22 (2012) 24509–24521.
- [49] A. Ajmal, I. Majeed, R.N. Malik, H. Idriss, M.A. Nadeem, *RSC Adv.* 4 (2014) 37003–37026.
- [50] Y. Wang, G.Z. Cao, *Adv. Mater.* 20 (2008) 2251–2269.
- [51] J.H. Huang, K.N. Ding, X.C. Wang, X.Z. Fu, *Langmuir* 25 (2009) 8313–8319.
- [52] G. Liu, P. Niu, L.C. Yin, H.M. Cheng, *J. Am. Chem. Soc.* 134 (2012) 9070–9073.